

Joint Channel Estimation and Cooperative Localization for Near-Field Ultra-Massive MIMO

Ruoxiao Cao, *Graduate Student Member, IEEE*, Hengtao He, *Member, IEEE*,
 Xianghao Yu, *Member, IEEE*, Shenghui Song, *Senior Member, IEEE*, Kaibin Huang, *Fellow, IEEE*,
 Jun Zhang, *Fellow, IEEE*, Yi Gong, *Senior Member, IEEE*, Khaled B. Letaief, *Fellow, IEEE*

Abstract—The next-generation (6G) wireless networks are expected to provide not only seamless and high data-rate communications, but also ubiquitous sensing services. By providing vast spatial degrees of freedom (DoFs), ultra-massive multiple-input multiple-output (UM-MIMO) technology is a key enabler for both sensing and communications in 6G. However, the adoption of UM-MIMO leads to a shift from the far field to the near field in terms of the electromagnetic propagation, which poses novel challenges in system design. Specifically, near-field effects introduce highly non-linear spherical wave models that render existing designs based on plane wave assumptions ineffective. In this paper, we focus on two crucial tasks in sensing and communications, respectively, i.e., localization and channel estimation, and investigate their joint design by exploring the near-field propagation characteristics, achieving mutual benefits between two tasks. In addition, multiple base stations (BSs) are leveraged to collaboratively facilitate a cooperative localization framework. To address the joint channel estimation and cooperative localization problem for near-field UM-MIMO systems, we propose a variational Newtonized near-field channel estimation (VNNCE) algorithm and a Gaussian fusion cooperative localization (GFCL) algorithm. The VNNCE algorithm exploits the spatial DoFs provided by the near-field channel to obtain position-related soft information, while the GFCL algorithm fuses this soft information to achieve more accurate localization. Additionally, we introduce a joint architecture that seamlessly integrates channel estimation and cooperative localization. Simulation results will demonstrate that the proposed VNNCE algorithm outperforms the state-of-the-art baseline, achieving channel estimation accuracy that approaches the Cramér–Rao lower bound (CRLB). Moreover, the joint architecture further enhances the performance by several dBs. It is also shown that the proposed GFCL algorithm significantly enhances localization accuracy, achieving millimeter-level precision compared to the meter-level accuracy of existing methods.

Index Terms—UM-MIMO; near-field; channel estimation; cooperative localization; soft information.

I. INTRODUCTION

The next-generation (6G) wireless networks are expected to enable various location-based services and applications,

Ruoxiao Cao is with the the Department of Electronic and Computer Engineering, The Hong Kong University of Science and Technology, Hong Kong SAR, and also with the Department of Electrical and Electronics Engineering, Southern University of Science and Technology, Shenzhen 518055, China. (e-mail: rcaoh@connect.ust.hk).

Hengtao He, Shenghui Song, Jun Zhang, and Khaled B. Letaief are with the the Department of Electronic and Computer Engineering, The Hong Kong University of Science and Technology, Hong Kong SAR. (e-mail: eehthe@ust.hk; eeshsong@ust.hk; eejzhang@ust.hk; eekhaled@ust.hk).

Xianghao Yu is with the Department of Electrical Engineering, City University of Hong Kong, Hong Kong SAR. (e-mail: alex.yu@cityu.edu.hk).

Kaibin Huang is with the Department of Electrical and Electronic Engineering, University of Hong Kong, Hong Kong SAR. (e-mail: huangk@eee.hku.hk).

Yi Gong is with the Department of Electrical and Electronics Engineering, Southern University of Science and Technology, Shenzhen 518055, China (e-mail: gongy@sustech.edu.cn).

such as Internet of Things (IoT) [1], unmanned aerial vehicles (UAVs) [2], and vehicle-to-everything (V2X) [3]. The attainment of high-accuracy localization over wireless networks will be one of the pivotal roles in 6G [4]. Traditionally, localization systems have been designed as independent components, which require a significant allocation of spectral resources and cause a huge waste of hardware cost. To solve the problem, a growing trend in future development is the integration of ubiquitous communication systems with localization capabilities, aiming to enhance spectral efficiency and reduce hardware costs [5]. The joint design of channel estimation and localization systems, such that they can share the same frequency band and hardware is currently attracting extensive research interest [6].

In the field of localization, two main categories can be identified: direct localization and indirect localization. Direct localization involves designing independent systems that directly estimate the user’s position based on the raw signals received by base stations (BSs) [7], [8]. However, such relatively independent direct localization does not meet our requirements for joint channel estimation and localization. In contrast, indirect localization algorithms rely on intermediate parameters, obtained from the communication systems, such as time-of-arrival (TOA) [9], angle-of-arrival (AOA) [10], and received signal strength (RSS) [11]. While indirect localization methods have provided paradigmatic attempts for joint design, the performance loss associated with single BS has become increasingly unacceptable.

To overcome this limitation, cooperative localization techniques have been developed to enhance the performance of indirect localization methods [12]. A sum-product algorithm was proposed in [12] to localize users in a distributed manner by exchanging messages, achieving significant performance gains compared to non-cooperative algorithms. Building on message passing methods, Meyer et al. [13] further presented a belief propagation (BP) algorithm for cooperative localization that completes the cooperative self-localization and distributed tracking task. Meanwhile, the concept of soft information was introduced in [14], including indications of estimation quality, such as the spatial distribution of the target position, which can have a positive impact on localization performance. However, these methods directly use a noisy measurement model instead of calculating position-related parameters, which are not acceptable in communication systems. In [6], a soft channel estimation and localization algorithm was proposed to leverage soft information to approach the theoretical limit of localization accuracy, but it relies on the traditional channel model that may not be suitable for 6G wireless networks.

The rapid development of 6G wireless networks has led to the emergence of ultra-massive multiple-input multiple-output

(UM-MIMO) technology [15], [16]. This technology equips BSs with hundreds or even thousands of antennas, enabling higher spectral and energy efficiency at the physical layer. However, the adoption of UM-MIMO leads to a shift from the far field to the near field in terms of the electromagnetic propagation [17]. In this scenario, it is necessary to employ the spherical wave model to accurately represent the propagation characteristics [18]. Unlike the planar wave model, the spherical wave model offers richer spatial degrees of freedom (DoFs) but also poses challenges due to its highly nonlinear form. These factors highlight the need for new approaches to address the challenges associated with near-field channel estimation and localization in UM-MIMO systems.

Existing near-field channel estimation approaches can typically be categorized into on-grid and off-grid methods. The on-grid methods [19] focus on designing a near-field codebook to incorporate both angle and distance parameters, making it difficult to achieve orthogonality and impacting the performance. Off-grid methods, although not requiring codebook orthogonality, struggle with achieving satisfactory results using existing optimization algorithms, such as the line search method [19] and the Newton's method [20]. In fact, the lack of convergence to the true solution in existing near-field channel estimation methods poses an unacceptable performance loss for localization systems. Thanks to the spatial DoFs provided by the spherical wave model, existing near-field localization approaches have significantly improved the performance of localization [21], [22], [23]. However, designing a joint channel estimation and cooperative localization algorithm for near-field UM-MIMO systems remains an open problem.

In this work, we propose a soft joint channel estimation and cooperative localization algorithm for UM-MIMO systems that can provide not only parameter estimates but also the corresponding confidence levels associated with these estimates. The proposed algorithm is specifically developed to tackle the challenges posed by the highly nonlinear spherical wave model in near-field channel estimation. Its objective is to achieve accurate and simultaneous channel estimation and localization in such scenarios. The main contributions are as follows:

- We propose a soft off-grid channel estimation algorithm for near-field UM-MIMO systems that is of low-complexity, tuning-free, and enjoys convergence guarantee. The proposed variational Newtonized near-field channel estimation (VNNCE) algorithm employs variational inference to transform the near-field channel estimation problem into an optimization problem. This approach utilizes a specially designed Newton gradient descent method for optimization. To ensure the convergence of the algorithm to the true solution, we introduce a novel near-field codebook that captures the unique characteristics of near-field channels and meets the requirements for convergence guarantee of the Newton's method.
- We present a soft cooperative localization algorithm for multiple-BS systems which is general, efficient, and robust. By leveraging the soft estimates obtained from the VNNCE algorithm, the proposed Gaussian fusion cooperative localization (GFCL) algorithm can not only infer the soft user position estimate based on a single BS, but also fuse them to obtain a new user position estimate with huge improvement of the localization accuracy. To further explore the potential of precise location estimation in channel estimation, we propose a joint architecture

that mutually enhances both channel estimation and cooperative localization. This joint architecture allows for a seamless integration of channel estimation and cooperative localization, unlocking new possibilities for enhanced wireless communication systems.

- The performance of the proposed algorithms are investigated via simulations. Simulation results demonstrate that the proposed VNNCE algorithm outperforms the state-of-the-art baseline in terms of channel estimation accuracy, and the parameter estimates approach the Cramér–Rao lower bound (CRLB). In a given practical system, the GFCL algorithm enhances the localization accuracy from the meter-level to the millimeter-level. Moreover, the exact localization provides additional gains for channel estimation in the proposed joint architecture to approach the theoretical limitation.

The rest of this paper is organized as follows. In Sec. II, we introduce the system model and the problem formulation. In Sec. III, the near-field soft channel estimation algorithm, i.e., the VNNCE algorithm, is provided. In Sec. IV, the requirement of the near-field codebook is derived. In Sec. V, the GFCL algorithm and the joint architecture are proposed. In Sec. VI, the simulation results are provided to illustrate the advantages of our proposed algorithm and architecture. Finally, we conclude the paper in Sec. VII.

Notations: For any matrix \mathbf{A} , \mathbf{A}^T , \mathbf{A}^{-1} and \mathbf{A}^H denote the transpose, inverse and conjugate transpose of \mathbf{A} , respectively. \mathbf{I}_M represents the identity matrix of size $N \times N$, and $\mathbf{1}_N$ and $\mathbf{0}_N$ are the N -dimensional all-ones and all-zeros vectors, respectively. A probability density function (PDF) is denoted by $p(\cdot)$. $\mathcal{N}(\mathbf{x}; \boldsymbol{\mu}, \boldsymbol{\Sigma})$ and $\mathcal{CN}(\mathbf{x}; \boldsymbol{\mu}, \boldsymbol{\Sigma})$ generates a random vector \mathbf{x} distributed according to a Gaussian PDF and a complex Gaussian PDF with mean vector $\boldsymbol{\mu}$ and covariance matrix $\boldsymbol{\Sigma}$, while $f_N(\mathbf{x}; \boldsymbol{\mu}, \boldsymbol{\Sigma})$ and $f_{CN}(\mathbf{x}; \boldsymbol{\mu}, \boldsymbol{\Sigma})$ represent their PDF. The angle of a complex number x is represented by $\angle x$. $\Re\{\cdot\}$ denotes the real part of the complex number. $F(\cdot)$ is the Fisher Information Matrix (FIM).

II. SYSTEM MODEL AND PROBLEM FORMULATION

In this section, we first introduce the received signal model and the spatial model for UM-MIMO systems. Then, we elaborate the near-field channel characteristic and formulate the joint channel estimation and cooperative localization problem.

A. Signal Model

We investigate an uplink time division duplexing based narrowband communication system consisting of a single-antenna user and I BSs¹. The carrier frequency is denoted as f , and the wavelength is represented as $\lambda = c/f$, where c is the speed of light. We assume that each BS employs a uniform linear array (ULA) with M antennas placed at an inter-element spacing of $d = \lambda/2$. The channel estimation for each BS is independent, so we consider an arbitrary BS without loss of generality and omit the superscript i . During the uplink training stage, the received signal $\mathbf{y} \in \mathbb{C}^M$ (observed variable or measurement) is given by

$$\mathbf{y} = \mathbf{h}x + \mathbf{n}, \quad (1)$$

¹The system can be effortlessly expanded to support multi-user scenarios or accommodate users with multiple antennas.

where $\mathbf{h} \in \mathbb{C}^M$ is the channel model, $x = 1$ is the pilot signal, and $\mathbf{n} \in \mathbb{C}^M$ is the additive complex noise. For ease of illustration, we assume $x = 1$.

In the conventional MIMO systems, users are assumed to be in the far-field region of the BS, where the channel is modeled under the planar wave assumption. Thus, the classical far-field channel \mathbf{h}^{far} is illustrated as

$$\mathbf{h}^{\text{far}} = \sum_{l=1}^L g_l e^{j\phi_l} \mathbf{a}(\theta_l), \quad (2)$$

where L is the number of paths. For each path l , $\theta_l \in (0, \pi)$ denotes the AoA, and $g_l e^{j\phi_l}$ is the complex path gain, where $g_l \in (0, \sqrt{p_t})$ and $\phi_l \in (0, 2\pi)$ are real numbers. We denote p_t as the transmit power. The far-field steering vector $\mathbf{a}(\theta_l)$ based on the planar wave assumption is given by

$$\mathbf{a}(\theta_l) = \left[1, e^{j\pi \cos \theta_l}, \dots, e^{j\pi(M-1) \cos \theta_l} \right]^T. \quad (3)$$

We can observe that the phase of each element in $\mathbf{a}(\theta_l)$ is linear with respect to the antenna index $m \in \{0, 1, \dots, M-1\}$. Thus, the far-field channel estimation problem can be treated as a line spectral estimation problem, and there are numerous existing studies working on it [24], [25], [26].

However, as future wireless networks are expected to be equipped with UM-MIMO, the planar wave model is no longer able to accurately describe the channel due to the change in the electromagnetic radiation field structure. As shown in Fig. 1(a), the radiation field is separated into two regions: near field and far field, by the Rayleigh distance [27], which is widely considered as the boundary between the two regions. The Rayleigh distance, given by $r_R = 2D^2/\lambda$, is related to the array aperture D and the carrier wavelength λ . From a physical perspective, the radiation field is considered far field and the far-field channel model can be approximated as the planar wave model (2) when the distance between the BS and the user or scatter is greater than r_R . It is important to note that if the distance is less than r_R , the radiation field is near field and the more accurate spherical wave model [22], [21] should be taken into account to characterize the near-field channel. For UM-MIMO systems, where $M \gg 1$, the array aperture of the ULA can be approximately given by $D \approx Md$, and thus the Rayleigh distance $r_R = M^2\lambda/2$ is proportional to M^2 . Therefore, in future UM-MIMO systems, the near-field region becomes non-negligible due to the increased number of antennas.

B. Spatial Model

Each BS i , where $i \in \{1, 2, \dots, I\}$ is the index of BS, receives uplink wireless signals through its ULA. The channel consists of one LoS path and several non-line-of-sight (NLoS) paths. It is important to note that the LoS path may be obstructed by obstacles such as walls. Fig. 1(b) illustrates an example scenario with one user, one scatter and $I = 3$ BSs. We observe that BS 1 receives one LoS path and one NLoS path, while BS 2 only receives one NLoS path due to the obstruction of the LoS path.

Let $\mathbf{x}_u = (x_u, y_u)^T$ denote the position vector of the user. For BS i , we have the known position vector $\mathbf{x}_b^i = (x_b^i, y_b^i)^T$ and the ULA rotation angle from the positive X-axis to the ULA direction, denoted as ω^i . Assuming the existence of the LoS path, the user's unknown position can be obtained using the spatial model:

$$\begin{bmatrix} x_u \\ y_u \end{bmatrix} = \begin{bmatrix} x_b^i \\ y_b^i \end{bmatrix} + r_{\text{LoS}}^i \begin{bmatrix} \cos(\theta_{\text{LoS}}^i + \omega^i) \\ \sin(\theta_{\text{LoS}}^i + \omega^i) \end{bmatrix}. \quad (4)$$

Therefore, if we have the propagation parameter estimate $(\hat{\theta}_{\text{LoS}}^i, \hat{r}_{\text{LoS}}^i)$ of the LoS path, the user position estimate $\hat{\mathbf{x}}_u = (\hat{x}_u, \hat{y}_u)^T$ can be obtained by using (1)(b).

C. Problem Formulation

As illustrated in Fig. 1(c), we consider the near-field channel model represented as:

$$\mathbf{h}^{\text{near}} = \sum_{l=1}^L g_l e^{j\phi_l} \mathbf{b}(\theta_l, r_l), \quad (5)$$

where $r_l \in (0, r_R)$ denotes the distance between the reference antenna of the ULA and the user or scatter. For simplicity, we consider a sample near-field channel with two paths in Fig. II(c), where r_1 and r_2 represent the direct path between the user and the BS and scattered path between the scatterer and the BS, respectively. Note that we ignore the amplitude variations across array antennas in (5) because it can be neglected when $r_l > 1.2D$ [28].

The main difference between the near-field channel (5) and far-field channel (2) lies in the steering vector $\mathbf{b}(\theta_l, r_l)$. Different from the far-field steering vector (3) based on the planar wave model, the near-field steering vector $\mathbf{b}(\theta_l, r_l)$ is derived from the spherical wave model given by

$$\mathbf{b}(\theta_l, r_l) = \left[e^{jk_c(r_{l,1}-r_l)}, \dots, e^{jk_c(r_{l,M}-r_l)} \right]^T, \quad (6)$$

where $k_c = 2\pi/c$ and $r_{l,m} = \sqrt{r_l^2 + \delta_m^2 d^2 + 2\delta_m d r_l \cos \theta_l}$ denote the wavenumber and the distance between the m th antenna of the ULA and the user or scatter of the l th path, respectively. The coefficient $\delta_m = \frac{2m-M+1}{2}$ represents the coordinate of the m th antenna. Unlike the planar wave model in the far field, the near-field spherical model indicates that the phase of each element in $\mathbf{b}(\theta_l, r_l)$ is nonlinear with respect to the antenna index m . Consequently, the energy of a near-field path is no longer concentrated at a single angle. Using only an angle parameter is inadequate for accurately describing the characteristics of the near-field path. Thus, for a BS located in the near field, the received pilot signal in (1) is given by²

$$\mathbf{y} = \mathbf{h} + \mathbf{n} = \sum_{l=1}^L g_l e^{j\phi_l} \mathbf{b}(\theta_l, r_l) + \mathbf{n}, \quad (7)$$

where the L -path channel \mathbf{h} is determined by unknown parameters $\boldsymbol{\mu} = \{\theta_l, r_l, g_l, \phi_l : l = 1, 2, \dots, L\}$, and the noise $\mathbf{n} \sim \mathcal{CN}(\mathbf{n}; \mathbf{0}_M, \sigma^2 \mathbf{I}_M)$ is assumed to be complex Gaussian noise with variance σ^2 . The objective of the soft channel estimation part is to provide reliable estimates of unknown parameters $\boldsymbol{\mu}$ and their confidence levels based on measurement \mathbf{y} for localization. The goal of the soft cooperative localization part is to infer the user's position by fusing these soft information from the soft channel estimation part, and use the more accurate user position estimate to improve the performance of channel estimation.

²We primarily consider a simplified denoising problem for convenience in this paper. Note that the proposed algorithm can be easily extended to the problem of compressive near-field channel estimation utilizing a similar idea from [29].

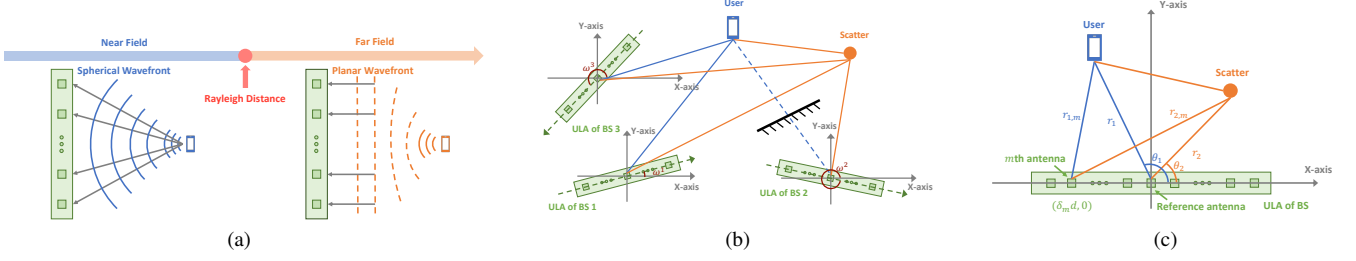


Fig. 1. (a) The near-field spherical model and far-field planar model. (b) A sample space model with three BSs. (c) A sample two-path near-field channel.

III. NEAR-FIELD SOFT CHANNEL ESTIMATION

In this section, we present a novel near-field channel estimation algorithm based on variational inference. The proposed VNNCE algorithm enables the estimation of channel parameters by modeling them as multivariate Gaussian distributions, providing soft estimates. Furthermore, we perform the CRLB analysis for near-field channel parameter estimation.

A. Bayesian Formulation

For simplicity, we take the estimation of a single path as an example, where $L = 1$ and omit the subscript l . The unknown channel parameters are denoted by $\boldsymbol{\mu} = (\theta, r, g, \phi)^T$. We aim to find the posterior PDF, given by:

$$p(\boldsymbol{\mu} | \mathbf{y}) = \frac{p(\mathbf{y}, \boldsymbol{\mu})}{p(\mathbf{y})}, \quad (8)$$

where the denominator $p(\mathbf{y})$, known as the model evidence, is the marginal probability of the joint PDF and acts as a normalizing constant. The joint PDF in the numerator (8) is the product of the prior PDF and the likelihood function, i.e.,

$$p(\mathbf{y}, \boldsymbol{\mu}) = p(\boldsymbol{\mu})p(\mathbf{y} | \boldsymbol{\mu}). \quad (9)$$

Since the noise \mathbf{n} is the independent identically distributed (iid) complex Gaussian distribution with zero mean and variance σ^2 , the likelihood function is given by

$$\begin{aligned} p(\mathbf{y} | \boldsymbol{\mu}) &= f_{\text{CN}}(\mathbf{y}; g e^{j\phi} \mathbf{b}(\theta, r), \sigma^2 \mathbf{I}_M) \\ &= \prod_{m=1}^M f_{\text{CN}}(y_m; g e^{j\phi} e^{jk_c(r_m - r)}, \sigma^2), \end{aligned} \quad (10)$$

where y_m represents the m th element of vector $\mathbf{y} \in \mathbb{C}^M$.

Unfortunately, obtaining analytical solutions for $\boldsymbol{\mu}$ is intractable. Therefore, we employ a type of approximation technique called variational inference to enable statistical inference of the intractable estimations [30]. The core idea of variational inference is to compute an approximate posterior PDF, denoted as the surrogate PDF, $q(\boldsymbol{\mu})$, which can approximate the true posterior PDF (8) well.

B. Variational Inference

According to the approximation inference theory [30], the logarithm of the model evidence $p(\mathbf{y})$ can be decomposed as

$$\ln p(\mathbf{y}) = \mathcal{D}_{\text{KL}}(q||p) + \mathcal{L}(q), \quad (11)$$

where $\mathcal{D}_{\text{KL}}(q||p)$ represents the Kullback-Leibler (KL) divergence between the surrogate PDF $q(\boldsymbol{\mu})$ and the true posterior PDF $p(\boldsymbol{\mu} | \mathbf{y})$. It is defined as

$$\mathcal{D}_{\text{KL}}(q||p) = - \int q(\boldsymbol{\mu}) \ln \left\{ \frac{p(\boldsymbol{\mu} | \mathbf{y})}{q(\boldsymbol{\mu})} \right\} d\boldsymbol{\mu}. \quad (12)$$

The functional $\mathcal{L}(q)$ is defined as

$$\mathcal{L}(q) = \int q(\boldsymbol{\mu}) \ln \left\{ \frac{p(\mathbf{y}, \boldsymbol{\mu})}{q(\boldsymbol{\mu})} \right\} d\boldsymbol{\mu} = \mathbb{E}_{q(\boldsymbol{\mu})} \left\{ \ln \frac{p(\mathbf{y}, \boldsymbol{\mu})}{q(\boldsymbol{\mu})} \right\}. \quad (13)$$

If we allow any possible choice for the surrogate PDF $q(\boldsymbol{\mu})$, the KL divergence will satisfy $\mathcal{D}_{\text{KL}}(q||p) \geq 0$, with equality if and only if, the surrogate PDF equals the posterior PDF $q(\boldsymbol{\mu}) = p(\boldsymbol{\mu} | \mathbf{y})$. Consequently, we obtain $\mathcal{L}(q) \leq \ln p(\mathbf{y})$ from (11), which means that $\mathcal{L}(q)$ is a lower bound on $\ln p(\mathbf{y})$. This lower bound is known as the evidence lower bound (ELBO). Although minimizing the KL divergence $\mathcal{D}_{\text{KL}}(q||p)$ is equivalent to maximizing $\mathcal{L}(q)$, working with the actual posterior PDF $p(\boldsymbol{\mu} | \mathbf{y})$ is generally intractable.

Therefore, we choose to evaluate a restricted family of candidate PDFs and search for the member within it that maximizes the $\mathcal{L}(q)$. Our principle is to restrict the family to only tractable PDFs while still allowing for sufficient adaptability to closely approximate the actual posterior PDF. To fulfill this principle, we restrict the surrogate PDF $q(\boldsymbol{\mu})$ to a multivariate (real) Gaussian distribution, i.e.,

$$q(\boldsymbol{\mu}) = f_{\text{N}}(\boldsymbol{\mu}; \hat{\boldsymbol{\mu}}, \hat{\mathbf{V}}_{\boldsymbol{\mu}}), \quad (14)$$

where $\boldsymbol{\mu} \sim \mathcal{N}(\boldsymbol{\mu}; \hat{\boldsymbol{\mu}}, \hat{\mathbf{V}}_{\boldsymbol{\mu}})$, $\hat{\boldsymbol{\mu}} = (\hat{\theta}, \hat{r}, \hat{g}, \hat{\phi})^T$ is the set of unobserved variable estimates, and the confidence level of the estimates $\hat{\mathbf{V}}_{\boldsymbol{\mu}}$ is given by

$$\hat{\mathbf{V}}_{\boldsymbol{\mu}} = \begin{bmatrix} \hat{v}_{\theta\theta} & \hat{v}_{\theta r} & \hat{v}_{\theta g} & \hat{v}_{\theta\phi} \\ \hat{v}_{\theta r} & \hat{v}_{rr} & \hat{v}_{rg} & \hat{v}_{r\phi} \\ \hat{v}_{\theta g} & \hat{v}_{rg} & \hat{v}_{gg} & \hat{v}_{g\phi} \\ \hat{v}_{\theta\phi} & \hat{v}_{r\phi} & \hat{v}_{g\phi} & \hat{v}_{\phi\phi} \end{bmatrix}.$$

The property of Gaussian distribution indicates that $\mathbb{E}_{q(\boldsymbol{\mu})} \{\ln q(\boldsymbol{\mu})\}$ is a constant, and ELBO is written as

$$\mathcal{L}(q) = \mathbb{E}_{q(\boldsymbol{\mu})} \{\ln p(\mathbf{y}, \boldsymbol{\mu})\} + \text{const}. \quad (15)$$

In practice, there is little or no knowledge about the channel information, such as location and fading. Hence, a flat prior is used in this non-informative condition with the least effect on outcomes of posterior inference [31]. The flat prior indicates a uniform prior where all values in the range are equally likely. To be specific, we assume $p(\boldsymbol{\mu}) = p(\theta)p(r)p(g)p(\phi)$, where $p(\theta) = 1/\pi$, $\theta \in (0, \pi)$, $p(r) = 1/r_R$, $r \in (0, r_R)$, $p(g) = 1/\sqrt{p_t}$, $g \in (0, \sqrt{p_t})$ and $p(\phi) = 1/2\pi$, $\phi \in (0, 2\pi)$. Under

this assumption, the prior PDF is not involved in the joint PDF (9), i.e.,

$$p(\mathbf{y}, \boldsymbol{\mu}) \propto \prod_{m=1}^M f_{\text{CN}} \left(y_m; g e^{j\phi} e^{jk_c(r_m-r)}, \sigma^2 \right). \quad (16)$$

By plugging the factor of joint PDF (16) into the ELBO (15) yields

$$\mathcal{L}(q) = \mathbb{E}_{q(\boldsymbol{\mu})} \left\{ \sum_{m=1}^M \ln f_{\text{CN}} \left(y_m; g e^{j\phi} e^{jk_c(r_m-r)}, \sigma^2 \right) \right\} + \text{const.} \quad (17)$$

For a complex Gaussian distribution $\mathcal{CN}(z; \mu_z, \sigma_z^2)$, its PDF can be represented as $f_{\text{CN}}(z; \mu_z, \sigma_z^2) = \frac{1}{\pi \sigma_z^2} e^{-\frac{(z-\mu_z)^2}{\sigma_z^2}}$. Based on (17), maximizing the ELBO is equivalent to maximizing

$$f(\boldsymbol{\mu}) = \sum_{m=1}^M 2|y_m|g \cos(\psi) - Mg^2, \quad (18)$$

where

$$\psi = k_c(r_m - r) + \phi - \angle y_m. \quad (19)$$

For the function $f(\boldsymbol{\mu})$, the first-order partial derivatives with (θ, r, g, ϕ) are

$$\frac{\partial f(\boldsymbol{\mu})}{\partial \theta} = \sum_{m=1}^M \frac{2k_c \delta_m d |y_m| g r}{r_m} \sin \psi, \quad (20a)$$

$$\frac{\partial f(\boldsymbol{\mu})}{\partial r} = \sum_{m=1}^M -2k_c |y_m| g \sin \psi \left(\frac{r - \delta_m d \cos \theta}{r_m} - 1 \right), \quad (20b)$$

$$\frac{\partial f(\boldsymbol{\mu})}{\partial g} = \sum_{m=1}^M 2|y_m| \cos \psi - 2Mg, \quad (20c)$$

$$\frac{\partial f(\boldsymbol{\mu})}{\partial \phi} = \sum_{m=1}^M -2|y_m| g \sin \psi. \quad (20d)$$

Our goal is to maximize the function $f(\boldsymbol{\mu})$ by updating $\boldsymbol{\mu}$, but updating the four parameters in $\boldsymbol{\mu}$ simultaneously is a formidable task. To reduce the burden of the optimization, we set the first-order derivatives (20c) and (20d) equal to zero, and find that the estimate of the complex channel gain that maximizes the function $f(\boldsymbol{\mu})$ is also the corresponding least squares (LS) solution, given by

$$\hat{g} e^{j\hat{\phi}} = \frac{\mathbf{b}(\theta, r)^H \mathbf{y}}{\|\mathbf{b}(\theta, r)\|^2}. \quad (21)$$

By replacing the channel gain $\hat{g} e^{j\hat{\phi}}$ with a fixed value (21) in the function $f(\boldsymbol{\mu})$ (18), we can derive that the estimate of the propagation parameters $(\hat{\theta}, \hat{r})$ are obtained as the solution to the subsequent optimization problem,

$$(\hat{\theta}, \hat{r}) = \arg \max_{\theta, r} G_{\mathbf{y}}(\theta, r), \quad (22)$$

where the cost function $G_{\mathbf{y}}(\theta, r)$ is given by

$$G_{\mathbf{y}}(\theta, r) = \frac{|\mathbf{b}(\theta, r)^H \mathbf{y}|^2}{\|\mathbf{b}(\theta, r)\|^2}. \quad (23)$$

C. Newton Gradient Descent for a Single Path

The Newton gradient descent method is utilized in our algorithm to maximize the function $f(\boldsymbol{\mu})$ by updating the estimate $\hat{\boldsymbol{\mu}}$ and its confidence level $\hat{\mathbf{V}}_{\boldsymbol{\mu}}$. Since the optimal solution for the gain parameters $(\hat{g}, \hat{\phi})$ is already given by (21), the Newton optimization step for estimate update is only applied to the position parameters $(\hat{\theta}, \hat{r})$. Specifically, we update the estimates as

$$(\hat{\theta}', \hat{r}')^T \triangleq (\hat{\theta}, \hat{r})^T - \ddot{f}^{-1}(\hat{\theta}, \hat{r}) \dot{f}(\hat{\theta}, \hat{r}), \quad (24)$$

where

$$\dot{f}(\theta, r) = \begin{bmatrix} \frac{\partial f(\boldsymbol{\mu})}{\partial \theta} \\ \frac{\partial f(\boldsymbol{\mu})}{\partial r} \end{bmatrix} \quad (25)$$

and

$$\ddot{f}(\theta, r) = \begin{bmatrix} \frac{\partial^2 f(\boldsymbol{\mu})}{\partial \theta^2} & \frac{\partial^2 f(\boldsymbol{\mu})}{\partial \theta \partial r} \\ \frac{\partial^2 f(\boldsymbol{\mu})}{\partial \theta \partial r} & \frac{\partial^2 f(\boldsymbol{\mu})}{\partial r^2} \end{bmatrix} \quad (26)$$

are the first-order partial derivative vector and the second-order partial derivative matrix of the function $f(\boldsymbol{\mu})$, respectively. The expressions for the first-order partial derivatives are defined in (20), and the second-order partial derivatives are shown in (27).

Algorithm 1 Near-Field Newton Gradient Descent

Input: Measurement \mathbf{y} , Original estimate $\hat{\boldsymbol{\mu}} = (\hat{\theta}, \hat{r}, \hat{g}, \hat{\phi})$;
 // Locally Concave Condition
 1: **if** $\ddot{f}(\hat{\theta}, \hat{r})$ is negative definite **then**
 2: Perform the Newton optimization step update in (24):
 $(\hat{\theta}', \hat{r}')^T \leftarrow (\hat{\theta}, \hat{r})^T - \ddot{f}^{-1}(\hat{\theta}, \hat{r}) \dot{f}(\hat{\theta}, \hat{r})$;
 // Near-Field Restriction Condition
 3: $\hat{r}' \leftarrow \min(\hat{r}', r_R)$;
 // Residual Energy Decrease Condition
 4: **if** $G_{\mathbf{y}}(\hat{\theta}, \hat{r}) > G_{\mathbf{y}}(\hat{\theta}', \hat{r}')$ **then**
 5: $(\hat{\theta}', \hat{r}') \leftarrow (\hat{\theta}, \hat{r})$;
 6: **end if**
 7: **else**
 8: $(\hat{\theta}', \hat{r}') \leftarrow (\hat{\theta}, \hat{r})$;
 9: **end if**
 10: Perform the corresponding LS solution in (21):

$$\hat{g}' e^{j\hat{\phi}'} \leftarrow \mathbf{b}(\hat{\theta}', \hat{r}')^H \mathbf{y} / M;$$

11: Perform the confidence level update in (28):

$$\hat{\mathbf{V}}'_{\boldsymbol{\mu}} \leftarrow -\mathbf{H}'^{-1};$$

Output: Updated estimate $\hat{\boldsymbol{\mu}}' = (\hat{\theta}', \hat{r}', \hat{g}', \hat{\phi}')$, Updated confidence level $\hat{\mathbf{V}}'_{\boldsymbol{\mu}}$.

The near-field Newton gradient descent procedure is illustrated in **Algorithm 1**. In addition to the general Newton optimization step described in Step 2, we have incorporated three near-field conditions to ensure that the optimization is conducted in the desired manner:

- 1) *Locally Concave:* Since the objective is to maximize the function $f(\boldsymbol{\mu})$, Step 1 specifies that the Newton optimization step (24) is performed only when the function is locally concave at $(\hat{\theta}, \hat{r})$, i.e., $\ddot{f}(\hat{\theta}, \hat{r})$ is negative definite.

$$\frac{\partial^2 f(\boldsymbol{\mu})}{\partial \theta^2} = \sum_{m=1}^M \frac{2k_c \delta_m^2 d^2 |y_m| g r^2}{r_m^2} \left(\frac{\sin \psi}{r_m} - k_c \cos \psi \right), \quad (27a)$$

$$\frac{\partial^2 f(\boldsymbol{\mu})}{\partial \theta \partial r} = \sum_{m=1}^M \frac{2k_c \delta_m d |y_m| g}{r_m} \left(k_c \left(\frac{r - \delta_m d \cos \theta}{r_m} - 1 \right) \cos \psi - \left(\frac{r^2 - \delta_m d r \cos \theta}{r_m^2} - 1 \right) \sin \psi \right), \quad (27b)$$

$$\frac{\partial^2 f(\boldsymbol{\mu})}{\partial \theta \partial g} = \sum_{m=1}^M \frac{2k_c \delta_m d |y_m| r}{r_m} \sin \psi, \quad \frac{\partial^2 f(\boldsymbol{\mu})}{\partial \theta \partial \phi} = \sum_{m=1}^M \frac{2k_c \delta_m d |y_m| g r}{r_m} \cos \psi. \quad (27c)$$

$$\frac{\partial^2 f(\boldsymbol{\mu})}{\partial r^2} = \sum_{m=1}^M 2k_c |y_m| g \left(\left(\frac{(r - \delta_m d \cos \theta)^2}{r_m^3} - \frac{1}{r_m} \right) \sin \psi - k_c \left(\frac{r - \delta_m d \cos \theta}{r_m} \right)^2 \cos \psi \right) \quad (27d)$$

$$\frac{\partial^2 f(\boldsymbol{\mu})}{\partial r \partial g} = \sum_{m=1}^M -2k_c |y_m| \left(\frac{r - \delta_m d \cos \theta}{r_m} - 1 \right) \sin \psi, \quad \frac{\partial^2 f(\boldsymbol{\mu})}{\partial r \partial \phi} = \sum_{m=1}^M -2k_c |y_m| g \left(\frac{r - \delta_m d \cos \theta}{r_m} - 1 \right) \cos \psi, \quad (27e)$$

$$\frac{\partial^2 f(\boldsymbol{\mu})}{\partial g^2} = -2M, \quad \frac{\partial^2 f(\boldsymbol{\mu})}{\partial g \partial \phi} = \sum_{m=1}^M -2 |y_m| \sin \psi, \quad \frac{\partial^2 f(\boldsymbol{\mu})}{\partial \phi^2} = \sum_{m=1}^M -2 |y_m| g \cos \psi. \quad (27f)$$

- 2) *Near-Field Restriction*: As the function $f(\boldsymbol{\mu})$ is derived from near-field model, it is essential to ensure that the estimated distance \hat{r} does not exceed the Rayleigh distance r_R . Step 3 introduces an additional rule to restrict the distance after the Newton optimization step.
- 3) *Residual Energy Decrease*: To guarantee the convergence of our algorithm, it is necessary to observe a decrease in the overall residual energy. Hence, Steps 4-6 specify that we only accept the update if the residual energy is non-increasing, i.e., the cost function in (23) is not less than the original.

In Step 10, after the Newton optimization step, the complex channel coefficient is updated using the LS solution in (21). Furthermore, since the surrogate PDF $q(\boldsymbol{\mu})$ is constrained to follow a multivariate Gaussian distribution (14), the update rule for the confidence level $\hat{\mathbf{V}}_{\boldsymbol{\mu}}$ is given by

$$\hat{\mathbf{V}}'_{\boldsymbol{\mu}} = -\mathbf{H}^{-1}, \quad (28)$$

where \mathbf{H} is the Hessian matrix. It is a square matrix consisting of the second-order partial derivatives of the scalar-valued function $f(\boldsymbol{\mu})$. Step 11 involves updating the confidence level with the Hessian matrix of the function $f(\hat{\theta}', \hat{r}', \hat{g}', \hat{\phi}')$.

In the preceding subsections of this section, we derived the Bayesian formulation, variational inference, and Newton gradient descent algorithm for the single-path case, i.e., $L = 1$. However, these methods are also effective in the multiple-path model. The general VNNCE Algorithm which is a direct extension of the single-path optimization to the multiple-path case will be discussed in the next subsection.

D. VNNCE Algorithm for Multiple Paths

In the multiple-path scenario, we denote the unknown channel parameters of the l th path as $\boldsymbol{\mu}_l = (\theta_l, r_l, g_l, \phi_l)^T$, and a set of unknown channel parameters for different paths as $\boldsymbol{\mu}_{1:k} = \{\theta_l, r_l, g_l, \phi_l : l = 1, 2, \dots, k\}$. Assuming that the first k paths have been estimated, the residual measurement corresponding to this set of unknown channel parameters is

$$\mathbf{y}_r(\boldsymbol{\mu}_{1:k}) = \mathbf{y} - \sum_{l=1}^k g_l e^{j\phi_l} \mathbf{b}(\theta_l, r_l). \quad (29)$$

As one of the off-grid estimation methods, we divide the estimation procedure into two stages: the on-grid detection stage and the off-grid refinement stage.

The detection stage aims to obtain a coarse estimate of the unknown channel parameters by restricting them to a discrete set, which serves as an initial guess for the refinement stage. We employ the orthogonal matching pursuit (OMP) algorithm [32] [33], one of the classical sparse recovery algorithms, to obtain a coarse estimate of the propagation parameters (θ, r) by constraining them to a two-dimensional (2D) finite discrete codebook Ω . The detailed structure of the codebook $\Omega = \{(\theta_{n_a}, r_{n_d}) : n_a = 1, 2, \dots, N_a, n_d = 1, 2, \dots, N_d\}$ will be elaborated in Sec. IV. For the l th path corresponding to the residual measurement, the coarse estimate $(\hat{\theta}_l, \hat{r}_l)$ obtained by the OMP algorithm is given by

$$(\hat{\theta}_l, \hat{r}_l) = \arg \max_{(\theta, r) \in \Omega} |\mathbf{b}^H(\theta, r) \mathbf{y}_r(\boldsymbol{\mu}_{1:l-1})|^2, \quad (30)$$

which is equivalent to maximizing the cost function $G_{\mathbf{y}_r}(\theta, r)$ in (23). Subsequently, the corresponding complex channel coefficient can be obtained as $\hat{g}_l e^{j\hat{\phi}_l} = \mathbf{b}^H(\hat{\theta}_l, \hat{r}_l) \mathbf{y}_r(\boldsymbol{\mu}_{1:l-1}) / M$.

To address the estimation error introduced by the discrete estimates from the detection stage, the refinement stage is proposed to extend the Newton gradient descent from a single path to multiple paths. The refinement stage maximizes the ELBO over the continuum rather than discrete points, using the Newton gradient descent algorithm described in **Algorithm 1**. Given the fixed paths characterized by $\{(\hat{\boldsymbol{\mu}}_l, \hat{\mathbf{V}}_l), l = 1, 2, \dots, i-1, i+1, i+2, \dots, k\}$, the joint PDF of i th path's unknown channel parameters is given by

$$\begin{aligned} p(\mathbf{y}, \boldsymbol{\mu}_i) &\propto \prod_{m=1}^M f_{\text{CN}} \left(y_m; \Xi + g_i e^{j\phi_i} e^{jk_c(r_i, m - r_i)}, \sigma^2 \right) \\ &\propto \prod_{m=1}^M f_{\text{CN}} \left(y_m - \Xi; g_i e^{j\phi_i} e^{jk_c(r_i, m - r_i)}, \sigma^2 \right), \end{aligned} \quad (31)$$

Algorithm 2 Proposed VNNCE Algorithm

Input: Measurement \mathbf{y} , Numbers of rounds R_s and R_c , Number of channel paths L' ;

Initialization: $l \leftarrow 0$;

- 1: **while** $l < L'$ **do**
- 2: $l \leftarrow l + 1$;
- // Coarse Estimate
- 3: Perform the OMP algorithm in (30):

$$(\hat{\theta}_l, \hat{r}_l) \leftarrow \arg \max_{(\theta, r) \in \Omega} G_{\mathbf{y}_r(\boldsymbol{\mu}_{1:l-1})}(\theta, r);$$

- 4: Perform the corresponding least squares estimate in (21):

$$\hat{g}_l e^{j\hat{\phi}_l} \leftarrow \mathbf{b}(\hat{\theta}_l, \hat{r}_l)^H \mathbf{y}_r(\boldsymbol{\mu}_{1:l-1}) / M;$$

 // Single Refinement

- 5: Fixed $\hat{\boldsymbol{\mu}}_{1:l-1}$, i.e., we treat $\mathbf{y}_r(\hat{\boldsymbol{\mu}}_{1:l-1})$ as the measurement, refine R_s rounds of Near-field Newton gradient descent in Algorithm 1 on $\hat{\boldsymbol{\mu}}_l$ to obtain $\hat{\boldsymbol{\mu}}'_l$ and $\hat{\mathbf{V}}'_{\boldsymbol{\mu},l}$:

- 6: $\hat{\boldsymbol{\mu}}_{1:l} \leftarrow \hat{\boldsymbol{\mu}}_{1:l-1} \cup \{\hat{\boldsymbol{\mu}}'_l\}$, $\hat{\boldsymbol{\mu}}_l \leftarrow \hat{\boldsymbol{\mu}}'_l$, $\hat{\mathbf{V}}_{\boldsymbol{\mu},l} \leftarrow \hat{\mathbf{V}}'_{\boldsymbol{\mu},l}$;

 // Cyclic Refinement

- 7: **for** $i = 1 : R_c$ **do**

- 8: **for each** $\hat{\boldsymbol{\mu}}_k$ in $\hat{\boldsymbol{\mu}}_{1:l}$ **do**

- 9: Fixed $\hat{\boldsymbol{\mu}}_{1:k-1, k+1:l}$, i.e., we treat $\mathbf{y}_r(\boldsymbol{\mu}_{1:k-1, k+1:l})$ as the measurement, refine R_s rounds of Near-field Newton gradient descent in Algorithm 1 on $\hat{\boldsymbol{\mu}}_k$ to obtain $\hat{\boldsymbol{\mu}}'_k$ and $\hat{\mathbf{V}}'_{\boldsymbol{\mu},k}$:

- 10: $\hat{\boldsymbol{\mu}}_{1:l} \leftarrow \hat{\boldsymbol{\mu}}_{1:k-1} \cup \{\hat{\boldsymbol{\mu}}'_k\} \cup \hat{\boldsymbol{\mu}}_{k+1:l}$, $\hat{\boldsymbol{\mu}}_k \leftarrow \hat{\boldsymbol{\mu}}'_k$, $\hat{\mathbf{V}}_{\boldsymbol{\mu},k} \leftarrow \hat{\mathbf{V}}'_{\boldsymbol{\mu},k}$;

- 11: **end for**

- 12: **end for**

- 13: **end while**

Output: Estimated result of channel parameters and their confidence levels $\{\hat{\boldsymbol{\mu}}_l, \hat{\mathbf{V}}_{\boldsymbol{\mu},l} : l = 1, 2, \dots, L'\}$.

where Ψ is the sum of all fixed channel, i.e.,

$$\Xi = \sum_{l=1, l \neq i}^k g_l e^{j\phi_l} e^{jk_c(r_{l,m} - r_l)}. \quad (32)$$

The joint PDF (31) shows that $y_m - \Psi$, which is distributed according to a complex Gaussian PDF, represents the m th element of the vector $\mathbf{y}_r(\boldsymbol{\mu}_{1:i-1, i+1:k})$. Therefore, the Newton gradient descent in the multiple-path case can be performed similarly to the single-path case, as discussed in Sec. III-C.

The complete VNNCE algorithm for the multi-path case is summarized in **Algorithm 2**. The main components of the algorithm are discussed as follows:

- 1) *Coarse Estimate*: As mentioned in the detection stage, Steps 3 and 4 provide the coarse estimates as the initial guess for optimization.
- 2) *Single Refinement*: In Step 5, R_s rounds of near-field Newton gradient descent are utilized to refine $\hat{\boldsymbol{\mu}}_l$ and $\hat{\mathbf{V}}_{\boldsymbol{\mu},l}$ of the l th path.
- 3) *Cyclic Refinement*: In Steps 7-12, R_c rounds of *Single Refinement* are employed for further refinements. Unlike conventional forward algorithms, this step provides feedback for optimization to achieve fast convergence and high estimation accuracy.

E. Cramér-Rao Lower Bound

The CRLB is a type of tool for performance analysis that provides lower bounds on the variance of estimators. In this case, we consider parameter estimation in an additive white Gaussian noise (AWGN) scenario, where the noisy observation vector \mathbf{y} can be described as

$$\mathbf{y} = \mathbf{s}(\boldsymbol{\mu}) + \mathbf{z}, \quad (33)$$

with $\mathbf{z} \sim \mathcal{CN}(\mathbf{z}; \mathbf{0}_M, \sigma^2 \mathbf{I}_M)$. Here, $\boldsymbol{\mu} \in \mathbb{R}^L$ is the vector of all estimated parameters and $\mathbf{s}(\boldsymbol{\mu}) \in \mathbb{C}^M$ represents the differentiable manifold. Let weight vector $\boldsymbol{\alpha} \in \mathbb{R}^L$. We assume an unbiased estimate of $\boldsymbol{\alpha}^T \boldsymbol{\mu}$ as $\boldsymbol{\alpha}^T \hat{\boldsymbol{\mu}}(\mathbf{y})$. The variance of the estimator, given by $\mathbb{E}_{\mathbf{y}|\boldsymbol{\mu}} (\boldsymbol{\alpha}^T \hat{\boldsymbol{\mu}}(\mathbf{y}) - \boldsymbol{\alpha}^T \boldsymbol{\mu})^2$, is lower bounded by $\boldsymbol{\alpha}^T \mathbf{F}^{-1}(\boldsymbol{\mu}) \boldsymbol{\alpha}$. The (i, j) th element in FIM is obtained as

$$F_{i,j}(\boldsymbol{\mu}) = \mathbb{E}_{\mathbf{y}|\boldsymbol{\mu}} \left\{ \frac{\partial \ln p(\mathbf{y} | \boldsymbol{\mu})}{\partial \mu_i} \frac{\partial \ln p(\mathbf{y} | \boldsymbol{\mu})}{\partial \mu_j} \right\}. \quad (34)$$

For the AWGN scenario in (33), (34) can be simplified to

$$F_{i,j}(\boldsymbol{\mu}) = \frac{2}{\sigma^2} \Re \left\{ \left(\frac{\partial \mathbf{s}(\boldsymbol{\mu})}{\partial \mu_i} \right)^H \frac{\partial \mathbf{s}(\boldsymbol{\mu})}{\partial \mu_j} \right\}. \quad (35)$$

In the parameter estimation problem in (7), $\boldsymbol{\mu}$ consists of $\{\theta_l, r_l, g_l, \phi_l : l = 1, 2, \dots, L\}$, and $\mathbf{s}(\boldsymbol{\mu}) = \mathbf{h} = \sum_{l=1}^L \mathbf{h}_l = \sum_{l=1}^L g_l e^{j\phi_l} \mathbf{b}(\theta_l, r_l)$. For each l th single path, the m th element of first-order derivatives are

$$v_{\theta_l}^m = g_l e^{j\phi_l} e^{jk_c(r_{l,m} - r_l)} \times \frac{jk_c \delta_m d r_l \sin \theta_l}{r_{l,m}}, \quad (36a)$$

$$v_{r_l}^m = g_l e^{j\phi_l} e^{jk_c(r_{l,m} - r_l)} \times \frac{jk_c(r_l - \delta_m d \cos \theta_l - r_{l,m})}{r_{l,m}}, \quad (36b)$$

$$v_{g_l}^m = e^{j\phi_l} e^{jk_c(r_{l,m} - r_l)}, \quad (36c)$$

$$v_{\phi_l}^m = j g_l e^{j\phi_l} e^{jk_c(r_{l,m} - r_l)}. \quad (36d)$$

$\mathbf{F}(\boldsymbol{\mu})$ is formed by (35), and the CRLB of $\{\theta_l, r_l, g_l, \phi_l : l = 1, 2, \dots, L\}$ are given by the diagonal elements of $\mathbf{F}^{-1}(\boldsymbol{\mu})$.

IV. CODEBOOK DESIGN

In this section, we derive the requirement of the near-field codebook Ω design at the detection stage, so as to guarantee that the Newton gradient descent can converge to the true maximum of the cost function (23). Our proposal involves the design of a new near-field codebook, which is constructed by a collection of near-field steering vectors $\mathbf{b}(\theta, r)$ (codewords), where both the angles θ and distances r are sampled from the angle-distance domain. By incorporating both angle and distance parameters, our new near-field codebook aims to capture the complex characteristics of near-field channels more accurately.

Our primary objective is to ensure that the codebook generated by our NNCE algorithm serves as an appropriate initial guess for the Newton gradient descent method, enabling it to converge to the true solution.

Claim 1. For any function $f(x)$, we assume the initial guess x_0 falls within an interval $I = [x_t - \epsilon_0, x_t + \epsilon_0]$ around the true solution x_t where ϵ_0 is a constant and $f'(x_t) = 0$. As mentioned in [34], the Newton gradient descent method guarantees local convergence to the true solution x_t , if the following three conditions are satisfied:

- 1) $\forall x \in I, f''(x) \neq 0$;
- 2) $\forall x \in I, f'''(x)$ is continuous;
- 3) Given $M \triangleq \frac{1}{2}(\sup_{x \in I} |f''''(x)|)(\sup_{x \in I} |1/f''(x)|)$, $|\epsilon_0| < 1/M$.

For convenience, consider a single-path case as an example. We assume the complex channel gain, angle and distance are $g_t e^{j\phi_t}$, θ_t and r_t , respectively. The received signal here can be expressed as $\mathbf{y} = g_r e^{j\phi_r} \mathbf{b}(\theta_t, r_t)$. Note that the optimization problem in (22) is equivalent to

$$\arg \max_{\theta, r} \left| \frac{1}{M} \sum_{\delta_m} e^{jk(r_m - r_{t,m})} \right|. \quad (37)$$

Thus, we can denote the optimization problem as $\arg \max_{\theta, r} s(\theta, r)$. By using the second-order approximation of $r_m = r + \delta_m d \cos \theta + \frac{\delta_m^2 d^2 \sin^2 \theta}{2r}$, we can obtain

$$s(\theta, r) \approx \left| \frac{1}{M} \sum_{\delta_m} e^{j\delta_m \pi (\cos \theta - \cos \theta_t) + jk\delta_m^2 d^2 \left(\frac{\sin^2 \theta}{2r} - \frac{\sin^2 \theta_t}{2r_t} \right)} \right|. \quad (38)$$

In fact, this complex form is still difficult to obtain the requirement of the near-field codebook design. We observe that the first term dominates the value of $s(\theta, r)$, which is also supported by the Taylor expansion theory. From a physical perspective, the effect of angles of codewords on the cost function is crucial. When the codewords share the same angle, the influence of distance becomes more significant. Therefore, we will proceed to address these two items separately.

A. Angle Domain in the Near-Field Codebook

When considering the codewords with different angles, we focus on the contribution of the first term of (38), denoted as $s_1(\theta, r) = \left| \frac{1}{M} \sum_{\delta_m = -\frac{M-1}{2}}^{\frac{M-1}{2}} e^{j\delta_m \pi (\cos \theta - \cos \theta_t)} \right|$. When $M \gg 1$, this term can be approximated as

$$s_1(\theta, r) \approx \left| \frac{1}{\pi \alpha} \int_{t=-\alpha}^{\alpha} e^{jt} dt \right| = s_1(\alpha) = \left| \frac{\sin(\pi \alpha)}{\pi \alpha} \right|, \quad (39)$$

where $\alpha = \frac{1}{2}M(\cos \theta - \cos \theta_t)$. From the Fig. 2(a), which illustrates the function $s_1(\alpha)$ and its derivatives around the true solution $\alpha_t = 0$, we can observe that the first two conditions in **Claim 1** are satisfied when $\epsilon_0 < 0.66$. After necessary mathematical calculations, we can obtain $\epsilon_0 < 0.45$ is the sufficient condition of the third condition in **Claim 1**. Thus, the maximum acceptable grid spacing Δ_α of α is about 0.9. In general, for different codewords in the codebook, the cosine of angle $\cos \theta$ should be uniformly sampled as

$$\cos \theta_{n_\theta} = \frac{2n_\theta \Delta_\alpha - M + 1}{M}, \quad n_\theta = 0, 1, \dots, \left\lfloor \frac{M}{\Delta_\alpha} \right\rfloor - 1. \quad (40)$$

B. Distance Domain in the Near-Field Codebook

When considering the codewords with the same angle, the significance of the second item in (38) becomes prominent. We denote it as $s_2(\theta, r) = \left| \frac{1}{M} \sum_{\delta_m} e^{jk\delta_m^2 d^2 \left(\frac{\sin^2 \theta}{2r} - \frac{\sin^2 \theta_t}{2r_t} \right)} \right|$. Without loss of generality, we assume that there is a series of codewords can well describe the true angle, i.e., $\theta = \theta_t$ and $s_2(\theta, r) = \left| \frac{1}{M} \sum_{\delta_m} e^{j\frac{k\delta_m^2 d^2 \sin^2 \theta}{2} \left(\frac{1}{r} - \frac{1}{r_t} \right)} \right|$. In practice, this is

equivalent to designing the distance parameters for codewords with the same angle in the near-field codebook. We introduce the Fresnel functions to approximate the intricate function as [19]

$$s_2(\theta, r) \approx s_2(\beta) = \begin{cases} \left| \frac{C(\sqrt{\beta}) + jS(\sqrt{\beta})}{\sqrt{\beta}} \right| & \beta > 0 \\ \left| \frac{C(\sqrt{-\beta}) + jS(\sqrt{-\beta})}{\sqrt{-\beta}} \right| & \beta < 0 \end{cases}, \quad (41)$$

where $\beta = \frac{M^2 d^2 \sin^2 \theta}{2\lambda} \left(\frac{1}{r} - \frac{1}{r_t} \right)$. The Fresnel sine and cosine integral function are $S(x) = \int_0^x \sin(\frac{\pi}{2} t^2) dt$ and $C(x) = \int_0^x \cos(\frac{\pi}{2} t^2) dt$, respectively. From Fig. 2(b), which illustrates the function $s_2(\beta)$ and its derivatives around the true solution is $\beta_t = 0$, the first two conditions in **Claim 1** can be met when $\epsilon_0 < 2.08$. We can know that the third condition in **Claim 1** will be satisfied when $\epsilon_0 < 1.49$ with some mathematical manipulations, and the acceptable grid spacing Δ_β of β is $\Delta_\beta < 2.98$. Therefore, for those codewords with the same angle parameter θ in the codebook, the reciprocal of distance parameter $\frac{1}{r}$ should be uniformly sampled as

$$\frac{1}{r_{n_r}} = \frac{2n_r \lambda \Delta_\beta}{M^2 d^2 \sin^2 \theta}, \quad n_r = 1, 2, 3, \dots \quad (42)$$

Please note that the range of r should be limited to $(1.2D, r_R]$. If $r > r_R$ when $n_r = 1$, we select the codeword with (θ, r_R) as the only codeword in the codebook with the angle θ .

V. NEAR-FIELD SOFT COOPERATIVE LOCALIZATION

In this section, we present a novel cooperative localization algorithm based on Gaussian fusion. The GFCL algorithm utilizes the propagation parameter estimates provided by the VNNCE algorithm to obtain soft user positions for each BS. It then employs an appropriate strategy to fuse these soft positions, thereby enhancing the accuracy of the localization process. Furthermore, we propose a joint architecture that mutually enhances both channel estimation and cooperative localization.

A. Soft Relative Position

According to the spatial model (4), the relative position between the user or scatter and each BS (the superscript of BS index i and the subscript of path index l are omitted) can be represented as

$$\begin{bmatrix} x_r \\ y_r \end{bmatrix} = r \begin{bmatrix} \cos(\theta + \omega) \\ \sin(\theta + \omega) \end{bmatrix}. \quad (43)$$

Furthermore, the expressions for the propagation parameters can be easily obtained using the relative position parameters. They are given by

$$r = \sqrt{x_r^2 + y_r^2}, \quad (44)$$

$$\theta = \arccot \left(\frac{x_r \cos(\omega) + y_r \sin(\omega)}{y_r \cos(\omega) - x_r \sin(\omega)} \right). \quad (45)$$

With soft channel estimation, we can obtain the Gaussian representation of the propagation parameters. In fact, the propagation parameters are position parameters in a polar coordinate system with the BS as the origin. However, for cooperative localization, it is more suitable to work with the relative position parameters, which are the position parameters in a unified Cartesian coordinate system. Similar to the

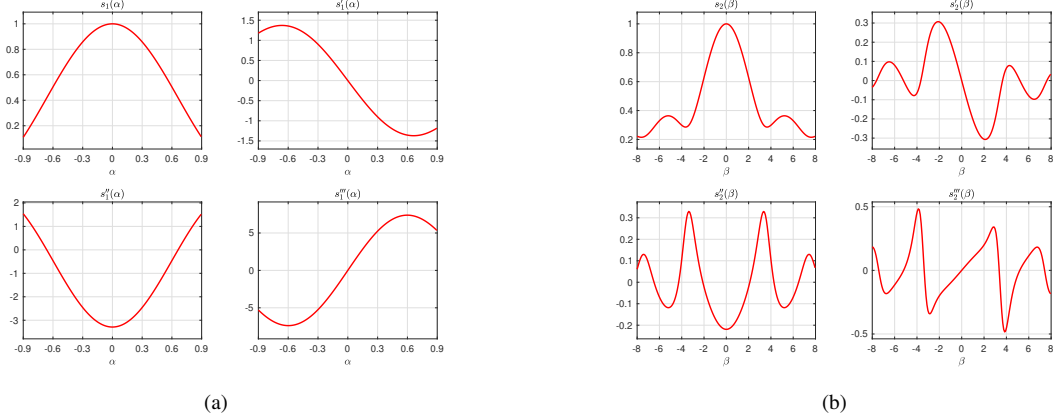


Fig. 2. (a) The first term $s_1(\alpha)$ and its derivatives. (b) The second term $s_2(\beta)$ and its derivatives.

propagation parameters, the relative position parameters can also be expressed in Gaussian form, given by

$$\boldsymbol{\nu} \sim \mathcal{N}(\boldsymbol{\nu}; \hat{\boldsymbol{\nu}}, \hat{\mathbf{V}}_{\boldsymbol{\nu}}), \quad (46)$$

where $\hat{\boldsymbol{\nu}} = (\hat{x}_r, \hat{y}_r)^T$ is the relative position estimate, and $\hat{\mathbf{V}}_{\boldsymbol{\nu}} = \begin{bmatrix} \hat{v}_{x_r x_r} & \hat{v}_{x_r y_r} \\ \hat{v}_{x_r y_r} & \hat{v}_{y_r y_r} \end{bmatrix}$ represents its confidence level. The relative parameter estimate can be obtained by substituting the propagation parameter estimate into (43), while determining the confidence level may present some challenges.

Claim 2. Let $y = f(u)$ and $u = g(x)$. If $h(x) = f(g(x))$ for every x , then the second derivative, using *Faà di Bruno's formula*, can be expressed as

$$\frac{d^2 y}{dx^2} = \frac{d^2 y}{du^2} \left(\frac{du}{dx} \right)^2 + \frac{dy}{du} \frac{d^2 u}{dx^2}. \quad (47)$$

To determine the matrix $\hat{\mathbf{V}}_{\boldsymbol{\mu}}$ in (28), we need to compute the second-order partial derivatives of the optimization function (18), which is given by

$$\ddot{f}(x_r, y_r) = \begin{bmatrix} \frac{\partial^2 f(\boldsymbol{\mu})}{\partial x_r^2} & \frac{\partial^2 f(\boldsymbol{\mu})}{\partial x_r \partial y_r} \\ \frac{\partial^2 f(\boldsymbol{\mu})}{\partial x_r \partial y_r} & \frac{\partial^2 f(\boldsymbol{\mu})}{\partial y_r^2} \end{bmatrix}. \quad (48)$$

However, directly substituting (44) and (45) into (18) can be a complex task. To simplify this process, we can utilize **Claim 2** to obtain the second-order partial derivatives as

$$\begin{aligned} \frac{\partial^2 f(\boldsymbol{\mu})}{\partial x_r^2} &= \left(\frac{\partial \theta}{\partial x_r} \right)^2 \frac{\partial^2 f(\boldsymbol{\mu})}{\partial \theta^2} + \frac{\partial^2 \theta}{\partial x_r^2} \frac{\partial f(\boldsymbol{\mu})}{\partial \theta} \\ &+ \left(\frac{\partial r}{\partial x_r} \right)^2 \frac{\partial^2 f(\boldsymbol{\mu})}{\partial r^2} + \frac{\partial^2 r}{\partial x_r^2} \frac{\partial f(\boldsymbol{\mu})}{\partial r}, \end{aligned} \quad (49a)$$

$$\begin{aligned} \frac{\partial^2 f(\boldsymbol{\mu})}{\partial y_r^2} &= \left(\frac{\partial \theta}{\partial y_r} \right)^2 \frac{\partial^2 f(\boldsymbol{\mu})}{\partial \theta^2} + \frac{\partial^2 \theta}{\partial y_r^2} \frac{\partial f(\boldsymbol{\mu})}{\partial \theta} \\ &+ \left(\frac{\partial r}{\partial y_r} \right)^2 \frac{\partial^2 f(\boldsymbol{\mu})}{\partial r^2} + \frac{\partial^2 r}{\partial y_r^2} \frac{\partial f(\boldsymbol{\mu})}{\partial r}, \end{aligned} \quad (49b)$$

$$\begin{aligned} \frac{\partial^2 f(\boldsymbol{\mu})}{\partial x_r \partial y_r} &= \frac{\partial \theta}{\partial x_r} \frac{\partial \theta}{\partial y_r} \frac{\partial^2 f(\boldsymbol{\mu})}{\partial \theta^2} + \frac{\partial^2 \theta}{\partial x_r \partial y_r} \frac{\partial f(\boldsymbol{\mu})}{\partial \theta} \\ &+ \frac{\partial r}{\partial x_r} \frac{\partial r}{\partial y_r} \frac{\partial^2 f(\boldsymbol{\mu})}{\partial r^2} + \frac{\partial^2 r}{\partial x_r \partial y_r} \frac{\partial f(\boldsymbol{\mu})}{\partial r}. \end{aligned} \quad (49c)$$

The first- and second-order partial derivatives according to (θ, r) are provided in (20) and (27), respectively. The coefficients associated with these derivatives are given by

$$\frac{\partial \theta}{\partial x_r} = -\frac{y_r}{x_r^2 + y_r^2}, \quad \frac{\partial \theta}{\partial y_r} = \frac{x_r}{x_r^2 + y_r^2}, \quad (50a)$$

$$\frac{\partial r}{\partial x_r} = \frac{x_r}{\sqrt{x_r^2 + y_r^2}}, \quad \frac{\partial r}{\partial y_r} = \frac{y_r}{\sqrt{x_r^2 + y_r^2}}, \quad (50b)$$

$$\frac{\partial^2 \theta}{\partial x_r^2} = \frac{2x_r y_r}{(x_r^2 + y_r^2)^2}, \quad \frac{\partial^2 \theta}{\partial y_r^2} = \frac{2x_r y_r}{(x_r^2 + y_r^2)^2}, \quad (50c)$$

$$\frac{\partial^2 \theta}{\partial x_r \partial y_r} = \frac{y_r^2 - x_r^2}{(x_r^2 + y_r^2)^2}, \quad \frac{\partial^2 r}{\partial x_r^2} = \frac{y_r^2}{(\sqrt{x_r^2 + y_r^2})^3}, \quad (50d)$$

$$\frac{\partial^2 r}{\partial y_r^2} = \frac{x_r^2}{(\sqrt{x_r^2 + y_r^2})^3}, \quad \frac{\partial^2 r}{\partial x_r \partial y_r} = -\frac{x_r y_r}{(\sqrt{x_r^2 + y_r^2})^3}. \quad (50e)$$

Then, the confidence level can be calculated using

$$\hat{\mathbf{V}}_{\boldsymbol{\nu}} = -\ddot{f}(x_r, y_r)^{-1}. \quad (51)$$

Therefore, we can obtain the soft relative positions from each path. Additionally, by combining the known BS position \mathbf{x}_b , we can determine the soft user or scatter position using (4).

B. Soft Position Fusion

Because all of the soft positions are defined as Gaussian variables, we can utilize the rule of multiple Gaussian products, as presented in **Claim 3**, to fuse these positions.

Claim 3. Let

$$f_N(\mathbf{x}; \mathbf{m}_1, \mathbf{V}_1), f_N(\mathbf{x}; \mathbf{m}_2, \mathbf{V}_2), \dots, f_N(\mathbf{x}; \mathbf{m}_K, \mathbf{V}_K)$$

be K Gaussian PDFs with mean vectors $\mathbf{m}_1, \mathbf{m}_2, \dots, \mathbf{m}_K$ and covariance matrixes $\mathbf{V}_1, \mathbf{V}_2, \dots, \mathbf{V}_K$, respectively. Then, the product of these Gaussian PDFs is a scaled Gaussian, which is given by

$$\prod_{k=1}^K f_N(\mathbf{x}; \mathbf{m}_k, \mathbf{V}_k) = A f_N(\mathbf{x}; \mathbf{m}_u, \mathbf{V}_u), \quad (52)$$

where $\mathbf{V}_u = (\sum_{k=1}^K \mathbf{V}_k^{-1})^{-1}$, $\mathbf{m}_u = \mathbf{V}_u \sum_{k=1}^K \mathbf{V}_k^{-1} \mathbf{m}_k$ and A is a constant.

However, it is important to note that the rule of multiple Gaussian products holds true only when the soft positions come from the same target, such as the user. If the soft positions come from different targets, the fusion process will be destructive. Therefore, it becomes necessary to design a strategy to associate these soft positions appropriately. To determine the association of soft positions, we define the cost of a Gaussian variable $f_N(\mathbf{x}; \mathbf{m}, \mathbf{V})$ is the mean squared error, which is given by

$$E_{\mathbf{x}} \left\{ \|\mathbf{x} - \mathbf{m}\|_2^2 \right\} = \text{tr}(\mathbf{V}). \quad (53)$$

In the localization problem, we consider a more accurate estimate to have a lower cost.

First, our objective is to find the most probable LoS path among all the paths for each BS. UM-MIMO systems usually rely on high-frequency communication, which offer the advantage of reducing the size of antenna elements, allowing for a larger number of antennas to be placed within a limited area [4]. In high-frequency communication systems, the energy of the signal is primarily concentrated on the LoS path. Therefore, the LoS path will have the largest cost according to (23), and the soft position calculated from the LoS path will have the least cost according to (53). It predicates the LoS path is the first path which is extracted by VNNCE, if it exists. In practical environments, the LoS path may be blocked by barriers, resulting in the soft scatter position having the least cost. Additionally, in situations with poor wireless channel conditions, false estimates of propagation parameters may occur, leading to the soft user position being far from the actual position.

To address these challenges, we employ a consistency strategy [6] to determine whether each soft position contributes constructively or destructively to the final user localization. Given two soft positions $\nu_1 \sim \mathcal{N}(\nu_1; \hat{\nu}_1, \hat{\mathbf{V}}_{\nu_1})$ and $\nu_2 \sim \mathcal{N}(\nu_2; \hat{\nu}_2, \hat{\mathbf{V}}_{\nu_2})$, we calculate the consistency indicator as:

$$\eta = \begin{cases} 1, & (\hat{\nu}_1 - \hat{\nu}_2)^T (\hat{\mathbf{V}}_{\nu_1} + \hat{\mathbf{V}}_{\nu_2})^{-1} (\hat{\nu}_1 - \hat{\nu}_2) < \zeta^2 \\ 0, & \text{otherwise} \end{cases}, \quad (54)$$

where ζ , a tunable parameter, is the consistency threshold. If and only if $\eta = 1$, the two soft positions can be considered to represent the same position and can be fused together.

The GFCL algorithm, outlined in **Algorithm 3**, can be primarily divided into three steps, each serving the following purposes:

- 1) *Soft User Position Inference*: Steps 1-3 focus on determining the most probable soft user position for fusion, as discussed earlier.
- 2) *Soft User Position Association*: Steps 4-5 aim to extract the most accurate soft user position as the reference position. Then, in Step 6, the remaining soft user positions are associated with the reference position. This association process helps assess whether each soft user position contributes constructively or destructively to the final user position estimate. By considering these associations, we can evaluate the impact of each soft user position on the accuracy and reliability of the cooperative localization result.
- 3) *Soft User Position Fusion*: In Step 7, all the constructively associated soft user positions are fused to obtain

Algorithm 3 Proposed GFCL Algorithm.

Input: Propagation parameters $\{\mu_l^i \sim \mathcal{N}(\mu_l^i; \hat{\mu}_l^i, \hat{\mathbf{V}}_{\mu_l^i}) : i = 1, 2, \dots, I, l = 1, 2, \dots, L'_i\}$, Consistency threshold ζ ;

// Soft User Position Inference

- 1: Infer all of the soft relative position parameters $\{\nu_l^i \sim \mathcal{N}(\nu_l^i; \hat{\nu}_l^i, \hat{\mathbf{V}}_{\nu_l^i}) : i = 1, 2, \dots, I, l = 1, 2, \dots, L'_i\}$ by 43 and 51;
- 2: Select the soft relative position ν^i with the least cost for each BS i , and consider it as the soft relative position between the user and BS i :

$$\nu^i \leftarrow \arg \min_{\nu_l^i} \text{tr}(\hat{\mathbf{V}}_{\nu_l^i});$$

- 3: Substitute $\{\nu^i : i = 1, 2, \dots, I\}$ into (4), then we obtain the soft user positions $\{\nu_u^i : i = 1, 2, \dots, I\}$;

// Soft User Position Association

- 4: Reindex the I soft user positions in descending order of cost:

$$\text{tr}(\hat{\mathbf{V}}_{\nu_u^1}) < \text{tr}(\hat{\mathbf{V}}_{\nu_u^2}) < \dots < \text{tr}(\hat{\mathbf{V}}_{\nu_u^I});$$

- 5: Select the first soft user position ν_u^1 with least cost as the reference soft user position, and set $\eta^i = 1$;
 - 6: Calculate the consistency indicators $\{\eta^i : i = 2, \dots, I\}$ for $\{\nu_u^i : i = 2, \dots, I\}$ by (54);
- // Soft User Position Fusion
- 7: Fuse all soft user positions with $\eta^i = 1$ by using (52) to obtain the user position estimate $\hat{\mathbf{x}}_u$:

$$\hat{\mathbf{x}}_u \leftarrow \sum_{i=1, \eta^i=1}^I \hat{\mathbf{V}}_{\nu_u^i} \hat{\nu}_u^i \left(\sum_{i=1, \eta^i=1}^I \hat{\mathbf{V}}_{\nu_u^i} \right)^{-1};$$

Output: User position estimate $\hat{\mathbf{x}}_u$.

the final user position estimate. Notably, the cost of the Gaussian fusion result is lower than the costs of the individual Gaussian elements prior to fusion. This implies that the cooperative localization accuracy improves after fusion, providing a higher level of precision compared to the independent localization accuracy of a single BS.

C. Joint Design of channel estimation and localization

Unlike existing channel estimation algorithms that focus solely on estimating the channel or determining the propagation parameters independently, our VNNCE algorithm offers a unique advantage. It not only provides accurate estimates of the propagation parameters for the GFCL localization algorithm but also assigns confidence levels to these estimates, enabling effective position fusion. This integrated approach is referred to as channel estimation aided cooperative localization. In our cooperative localization system, we utilize the improved user localization result obtained through the GFCL algorithm to reconstruct the channel. By incorporating this refined position into the VNNCE algorithm, we can achieve a more precise channel estimation result. This process is known as cooperative localization enhanced channel estimation.

To facilitate this joint approach, we propose a comprehensive architecture for wireless networks called Joint Channel Estimation and Cooperative Localization. The workflow of this architecture is as follows:

TABLE I
CHANNEL ESTIMATION KEY SIMULATION PARAMETERS

Parameter	Value
Antenna number of ULAs	$M = 256$
Wavelength of carrier signals	$\lambda_c = 3 \text{ mm}$
Number of paths	$L = 3$
Number of single refinement rounds	$R_s = 5$
Number of cyclic refinement rounds	$R_c = 5$
Grid spacing of angles	$\Delta_\alpha = 0.5$
Grid spacing of distances	$\Delta_\beta = 1$

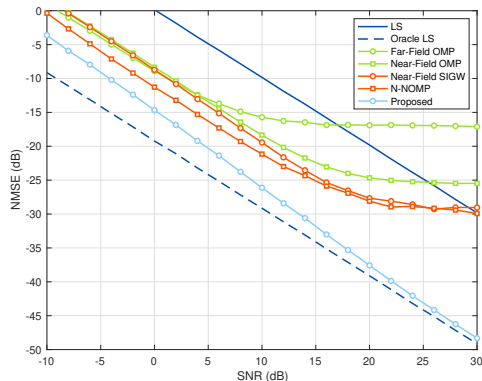


Fig. 3. NMSE achieved by different algorithms versus SNR.

- 1) *Channel Estimation*: We employ the VNNCE algorithm in parallel at each BS to estimate the channel parameters, including channel gain, angle, and distance. By using the received pilot signals, accurate estimates of these parameters are obtained, along with their associated confidence levels.
- 2) *Cooperative Localization*: The central server implements the GFCL algorithm, utilizing the estimated propagation parameters from Step 1, to perform user localization for each BS. By leveraging the localization results from multiple BSs, we can achieve accurate user position estimation through cooperative localization.
- 3) *Channel Refinement*: The more precise user position obtained in Step 2 is utilized to reconstruct the LoS channel and obtain the propagation parameters. With the LoS path parameters fixed, the VNNCE algorithm is once again employed at the BSs that have the LoS path. This step refines the channel estimation process, ensuring enhanced accuracy.

VI. SIMULATION RESULTS

In this section, we begin by presenting simulation results to assess the performance of the proposed VNNCE algorithm with respect to channel estimation. We conduct these simulations in a typical near-field single-BS UM-MIMO system. Following this, we proceed to evaluate the performance of propagation parameter estimation and cooperative localization in a practical near-field multiple-BS UM-MIMO system. Finally, we demonstrate the enhancement achieved in channel reconstruction.

We consider the normalized mean square error (NMSE) as the performance metric for channel estimation, which is defined as $\text{NMSE} = \mathbb{E}_{\hat{\mathbf{H}}} \left\{ \frac{\|\mathbf{H} - \hat{\mathbf{H}}\|_2^2}{\|\mathbf{H}\|_2^2} \right\}$. To conduct our simulations, we set the key parameters as listed in Table I. For each

TABLE II
LOCALIZATION SYSTEM ADDITIONAL KEY SIMULATION PARAMETERS

Parameter	Value
Number of BSs	$I = 4$
Positions of BSs	$\mathbf{x}_b^i = \{(0, 50), (20, 50), (50, 0), (50, 20)\}$
ULA rotations of BSs	$\omega^i = \{\pi, \pi, \pi/2, \pi/2\}$
Number of paths	$L^i = \{2, 2, 2, 2\}$
Noise variance	$\sigma^2 = -110 \text{ dBm}$
Consistency threshold	$\zeta = 3.5$

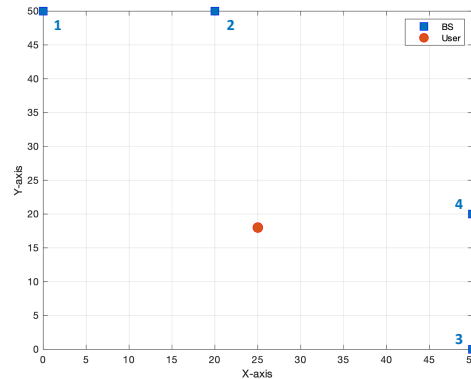


Fig. 4. Illustration of the near-field 4-BS UM-MIMO system in the simulation.

path, the angle $\theta_l \in (0, \pi)$ and distance $r_l \in (1.2D, r_R]$ are randomly and uniformly generated within the specified range. We compare the proposed VNNCE algorithm with several existing algorithms. The oracle LS method is considered as the NMSE performance bound, assuming perfect knowledge of the true angles and distances. The far-field OMP [35] and near-field OMP [19] are two on-grid algorithms, while the near-field SIGW [19] and N-NOMP [20] are two near-field off-grid channel estimation algorithms. As shown in Fig. 3, the proposed VNNCE algorithm significantly outperforms all the baselines in terms of NMSE performance at all considered SNR. We can observe that in the high SNR regimes, the performance of baselines no longer continues to linearly decrease as SNR increases, while our proposal can converge to the NMSE performance bound. This implies that our algorithm, compared to the baselines, can converge to the true solution in the high SNR regimes, thus demonstrating the effectiveness of our designed near-field codebook and algorithm.

To provide a more comprehensive evaluation of the parameter estimation performance of the VNNCE algorithm and the cooperative localization performance of the GFCL algorithm, we conducted a simulation using a practical near-field 4-BS UM-MIMO system. In this system, we assume the free space path loss model to generate the LoS channel. The channel gain of the LoS path is given by

$$g_{\text{LoS}} = \frac{\lambda\sqrt{P_t}}{4\pi r_{\text{LoS}}}. \quad (55)$$

Additionally, we generate a NLoS channel with random gain, angle, and distance. The gain of the NLoS path is less than one-third of the LoS path gain. We have included the additional key simulation parameters in Table II, while maintaining the other parameters as listed in Table I. The simulation scenario of the practical system is depicted in Fig. 4. It is important to note that due to the varying distances between

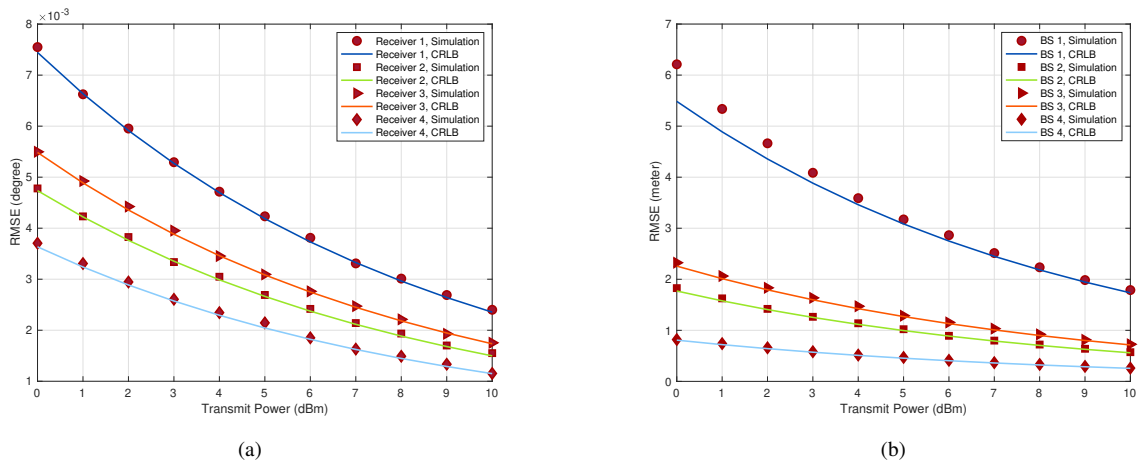


Fig. 5. (a) RMSE of the LoS path angle estimate $\hat{\theta}_{\text{LoS}}$. (b) RMSE of the LoS path distance estimate \hat{r}_{LoS} .

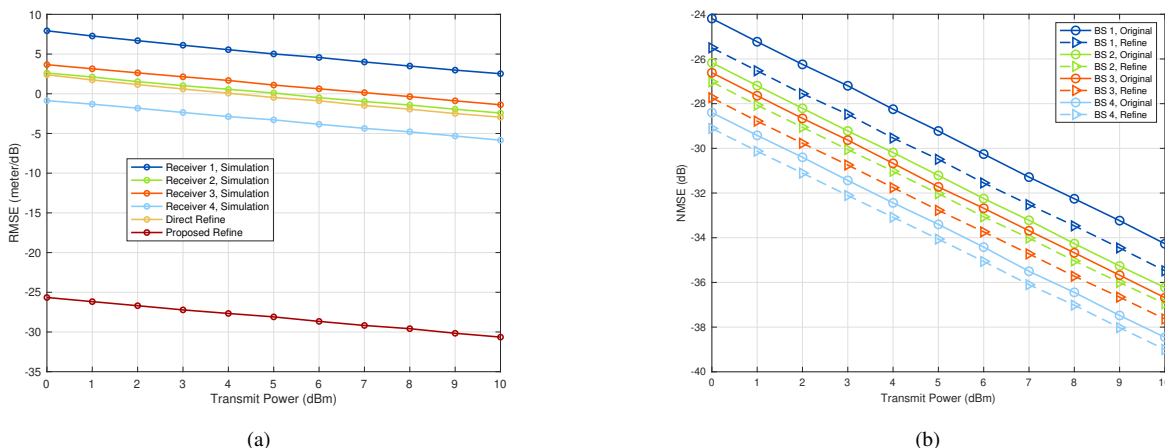


Fig. 6. (a) RMSE of soft cooperative localization through joint channel estimation and localization. (b) NMSE of soft channel estimation through joint channel estimation and localization.

each BS and the user, the received SNR at each BS differs, even for the same pilot signal.

Fig. 5(a) and Fig. 5(b) illustrate the root mean square error (RMSE) of the propagation parameter estimates of the LoS path, which is given by $\text{RMSE} = \sqrt{\mathbb{E}_{\hat{x}} \{(x - \hat{x})^2\}}$, specifically angle estimate and distance estimate. The proposed VNNCE algorithm is independently performed at each BS, while the CRLB is derived for each BS individually. In Fig. 5(a), we observe that the angle estimate achieved by the proposed VNNCE algorithm closely approaches the level of the CRLB across all signal-to-noise ratio (SNR) regimes. As discussed in Sec. IV, the angle parameter holds greater significance in the cost function, which results in the VNNCE algorithm attaining higher angular resolution compared to distance resolution. This conclusion is further supported by the results presented in Fig. 5(b). We observe that the performance of the distance estimate closely aligns with that of the angle estimate in high SNR levels. However, when the SNR is not sufficiently high, the distance estimate performance still exhibits a gap from the theoretical estimation limit. One noteworthy observation is that, despite BS 3 being closer to the user compared to BS 2, implying a higher received signal SNR at BS 3, the

estimation performance of both the angle and distance at BS 3 is inferior to that of BS 2. This discrepancy can be attributed to the uniform sampling of our codebook for $\cos \theta$, and the optimization algorithm's estimation of $\cos \theta$. As a result, the VNNCE algorithm achieves higher angular resolution near $\theta = \pi/2$ compared to other regions. The degradation in distance estimation performance primarily stems from the dependence on the angle estimation results, as evident in our codebook generation approach outlined in Sec. IV.

Fig. 6(a) displays the RMSE of localization performance using different collaborative approaches. The single BS i result indicates that the user is localized independently by BS i , thus the performance of independent localization should be equivalent to the result of distance estimation. In the case of most existing parameter estimation algorithms, they can only estimate the values of propagation parameters. Therefore, the conventional strategy for cooperative localization involves directly averaging the user positions obtained from different BSs. However, even with our proposed VNNCE algorithm, which is capable of achieving the CRLB, the performance of the conventional strategy may not reach the level of the best single BS localization. To provide a clearer representation of

the significant performance improvement brought about by our proposed VNNCE-aided GFSL algorithm, we employed the unit dBmeter. Using dBmeter allows for a better visualization and comparison of the performance gains achieved through our approach. From the comparison presented in Fig. 6(a), we can observe that our VNNCE aided GFSL algorithm has substantially enhanced the localization accuracy from the meter-level to the millimeter-level. This demonstrates the effectiveness of our approach in achieving highly precise and accurate user localization. Furthermore, the results underscore the necessity of variational inference in our high-precision localization system.

Fig. 6(b) compares the NMSE of the channel estimation performance for Steps 1 and 3 in the joint architecture, considering each BS individually. The results clearly demonstrate that the channel refinement step leads to a notable improvement of approximately 1.4 dB in the channel estimation accuracy for BS 1. By referring to Fig. 3, we can observe that this improvement enables the channel estimation results to closely approach the theoretical limit, i.e., the performance level of the oracle LS method. This signifies the effectiveness of the channel refinement process in enhancing the accuracy and quality of the channel estimation results, thereby bringing them closer to the theoretical limits of the system.

VII. CONCLUSION

In this paper, we proposed a soft joint channel estimation and cooperative localization algorithm for UM-MIMO systems in near-field scenarios. The proposed algorithm includes a low-complexity, tuning-free, and convergence-guaranteed variational Newtonized near-field channel estimation algorithm and a general, efficient, and robust Gaussian fusion cooperative localization algorithm. We also proposed a joint architecture that allows for a seamless integration of channel estimation and cooperative localization. Simulation results demonstrated that the proposed algorithm and architecture can significantly enhance the performance of near-field UM-MIMO.

REFERENCES

- [1] D. C. Nguyen, M. Ding, P. N. Pathirana, A. Seneviratne, J. Li, D. Niyato, O. Dobre, and H. V. Poor, "6G internet of things: A comprehensive survey," *IEEE Internet Things J.*, vol. 9, no. 1, pp. 359–383, Jan. 2021.
- [2] Y. Zeng, Q. Wu, and R. Zhang, "Accessing from the sky: A tutorial on UAV communications for 5G and beyond," *Proc. IEEE*, vol. 107, no. 12, pp. 2327–2375, Dec. 2019.
- [3] T. Luettel, M. Himmelsbach, and H.-J. Wuensche, "Autonomous ground vehicles-concepts and a path to the future," *Proc. IEEE*, vol. 100, no. Special Centennial Issue, pp. 1831–1839, Apr. 2012.
- [4] T. S. Rappaport, Y. Xing, O. Kanhere, S. Ju, A. Madanayake, S. Mandal, A. Alkhateeb, and G. C. Trichopoulos, "Wireless communications and applications above 100 GHz: Opportunities and challenges for 6G and beyond," *IEEE Access*, vol. 7, pp. 78 729–78 757, Jun. 2019.
- [5] A. Liu, Z. Huang, M. Li, Y. Wan, W. Li, T. X. Han, C. Liu, R. Du, D. K. P. Tan, J. Lu *et al.*, "A survey on fundamental limits of integrated sensing and communication," *IEEE Commun. Surv. Tutor.*, vol. 24, no. 2, pp. 994–1034, Feb. 2022.
- [6] X. Yang, C.-K. Wen, Y. Han, S. Jin, and A. L. Swindlehurst, "Soft channel estimation and localization for millimeter wave systems with multiple receivers," *IEEE Trans. Signal Process.*, vol. 70, pp. 4897–4911, Jul. 2022.
- [7] A. J. Weiss, "Direct position determination of narrowband radio frequency transmitters," *IEEE Signal Process. Lett.*, vol. 11, no. 5, pp. 513–516, Apr. 2004.
- [8] N. Garcia, H. Wymeersch, E. G. Larsson, A. M. Haimovich, and M. Coulon, "Direct localization for massive MIMO," *IEEE Trans. Signal Process.*, vol. 65, no. 10, pp. 2475–2487, Feb. 2017.
- [9] I. Guvenc and C.-C. Chong, "A survey on TOA based wireless localization and NLOS mitigation techniques," *IEEE Commun. Surv. Tutor.*, vol. 11, no. 3, pp. 107–124, Aug. 2009.

- [10] J. Yin, Q. Wan, S. Yang, and K. Ho, "A simple and accurate TDOA-AOA localization method using two stations," *IEEE Signal Process. Lett.*, vol. 23, no. 1, pp. 144–148, Jan. 2016.
- [11] G. Wang and K. Yang, "A new approach to sensor node localization using RSS measurements in wireless sensor networks," *IEEE Trans. Wireless Commun.*, vol. 10, no. 5, pp. 1389–1395, Mar. 2011.
- [12] H. Wymeersch, J. Lien, and M. Z. Win, "Cooperative localization in wireless networks," *Proc. IEEE*, vol. 97, no. 2, pp. 427–450, Feb. 2009.
- [13] F. Meyer, O. Hlinka, H. Wymeersch, E. Riegler, and F. Hlawatsch, "Distributed localization and tracking of mobile networks including noncooperative objects," *IEEE Trans. Signal Inf. Process. Netw.*, vol. 2, no. 1, pp. 57–71, Mar. 2016.
- [14] S. Mazuelas, A. Conti, J. C. Allen, and M. Z. Win, "Soft range information for network localization," *IEEE Trans. Signal Process.*, vol. 66, no. 12, pp. 3155–3168, Jan. 2018.
- [15] W. Yu, Y. Ma, H. He, S. Song, J. Zhang, and K. B. Letaief, "AI-native transceiver design for near-field ultra-massive MIMO: Principles and techniques," *arXiv preprint arXiv:2309.09575*, 2023.
- [16] R. Chataut and R. Akl, "Massive MIMO systems for 5G and beyond networks-overview, recent trends, challenges, and future research direction," *Sensors*, vol. 20, no. 10, p. 2753, May 2020.
- [17] W. Yu, Y. Shen, H. He, X. Yu, S. Song, J. Zhang, and K. B. Letaief, "An adaptive and robust deep learning framework for THz ultra-massive MIMO channel estimation," *IEEE J. Sel. Topics Signal Process.*, to appear.
- [18] W. Yu, H. He, X. Yu, S. Song, J. Zhang, and K. B. Letaief, "Blind performance prediction for deep learning based ultra-massive MIMO channel estimation," in *IEEE Int. Conf. Commun.*, May-Jun. 2023, pp. 2613–2618.
- [19] M. Cui and L. Dai, "Channel estimation for extremely large-scale MIMO: Far-field or near-field," *IEEE Trans. Commun.*, vol. 70, no. 4, pp. 2663–2677, Apr. 2022.
- [20] Z. Lu, Y. Han, S. Jin, M. Matthaiou, and T. Q. Quek, "Near-field channel reconstruction and user location for ELAA systems," in *Proc. Int. Symp. Wireless Commun. Syst. (ISWCS)*, Hangzhou, China, Oct. 2022.
- [21] F. Guidi and D. Dardari, "Radio positioning with EM processing of the spherical wavefront," *IEEE Trans. Wireless Commun.*, vol. 20, no. 6, pp. 3571–3586, Jun. 2021.
- [22] A. Guerra, F. Guidi, D. Dardari, and P. M. Djurić, "Near-field tracking with large antenna arrays: Fundamental limits and practical algorithms," *IEEE Trans. Signal Process.*, vol. 69, pp. 5723–5738, Aug. 2021.
- [23] R. Cao, H. He, X. Yu, J. Zhang, S. Song, Y. Gong, and K. B. Letaief, "Belief propagation for near-field cooperative localization and tracking in 6G vehicular networks," in *Proc. IEEE Int. Medit. Conf. Commun. and Netw. (MeditCom)*, Athens, Greece, Sept. 2022, pp. 160–165.
- [24] Z. Yang and L. Xie, "On gridless sparse methods for line spectral estimation from complete and incomplete data," *IEEE Trans. Signal Process.*, vol. 63, no. 12, pp. 3139–3153, Apr. 2015.
- [25] B. Mamandipoor, D. Ramasamy, and U. Madhow, "Newtonized orthogonal matching pursuit: Frequency estimation over the continuum," *IEEE Trans. Signal Process.*, vol. 64, no. 19, pp. 5066–5081, Oct. 2016.
- [26] M.-A. Badiu, T. L. Hansen, and B. H. Fleury, "Variational Bayesian inference of line spectra," *IEEE Trans. Signal Process.*, vol. 65, no. 9, pp. 2247–2261, Jan. 2017.
- [27] J. Kraus and R. Marhefka, *Antennas for All Applications*, ser. McGraw-Hill series in electrical engineering. McGraw-Hill, 2002. [Online]. Available: <https://books.google.com.hk/books?id=V6pSPgAACAAJ>
- [28] E. Björnson, Ö. T. Demir, and L. Sanguinetti, "A primer on near-field beamforming for arrays and reconfigurable intelligent surfaces," in *Proc. Conf. Rec. Asilomar Conf. Signals Syst. Comput.*, Pacific Grove, CA, USA, Oct.-Nov. 2021, pp. 105–112.
- [29] C. A. Metzler, A. Maleki, and R. G. Baraniuk, "From denoising to compressed sensing," *IEEE Trans. Inf. Theory*, vol. 62, no. 9, pp. 5117–5144, Sept. 2016.
- [30] C. M. Bishop and N. M. Nasrabadi, *Pattern recognition and machine learning*. Springer, 2006, vol. 4, no. 4.
- [31] A. Gelman, J. B. Carlin, H. S. Stern, and D. B. Rubin, *Bayesian data analysis*. Chapman and Hall/CRC, 1995.
- [32] S. G. Mallat and Z. Zhang, "Matching pursuits with time-frequency dictionaries," *IEEE Trans. Signal Process.*, vol. 41, no. 12, pp. 3397–3415, Dec. 1993.
- [33] W. U. Bajwa, J. Haupt, A. M. Sayeed, and R. Nowak, "Compressed channel sensing: A new approach to estimating sparse multipath channels," *Proc. IEEE*, vol. 98, no. 6, pp. 1058–1076, Jun. 2010.
- [34] U. M. Ascher and C. Greif, *A first course on numerical methods*. SIAM, 2011.
- [35] J. Rodríguez-Fernández, N. González-Prelcic, K. Venugopal, and R. W. Heath, "Frequency-domain compressive channel estimation for frequency-selective hybrid millimeter wave MIMO systems," *IEEE Trans. Wireless Commun.*, vol. 17, no. 5, pp. 2946–2960, May 2018.